Proceedings of the Combustion Institute 40 (2024) 105418

Contents lists available at ScienceDirect

Proceedings of the Combustion Institute

journal homepage: www.elsevier.com/locate/proci

Exploring nonlinear flame speed inhibition effects in mixtures of R1234yf and R32 under microgravity conditions☆

Raik Hesse [a,*], Roman Glaznev [a], Raymond Langer [a], Christian Schwenzer [a], Valeri Babushok [b], Gregory Linteris [b], Heinz Pitsch [a], Joachim Beeckmann [a]

[a] Institute for Combustion Technology, RWTH Aachen University, Templergraben 64, 52056 Aachen, Germany
[b] National Institute of Standards and Technology, Gaithersburg, MD, USA

ARTICLE INFO

Keywords:
Laminar flame speed
Refrigerant flammability
R32
R1234yf
Microgravity

ABSTRACT

This study investigates the flame speed inhibition effects in R1234yf and R32 mixtures, two hydrofluorocarbon (HFC) refrigerants with low global warming potential but mild flammability. The laminar flame speed ($S^0_{L,u}$) is a crucial parameter for assessing fire potential, and this research aims to provide high-fidelity flame speed data for refining chemical kinetic models. The slow flame propagation behavior of these refrigerants poses a formidable challenge to measurements due to buoyancy and radiation effects. This study simultaneously obtains $S^0_{L,u}$ data using optical (Schlieren) and pressure-rise methods under microgravity conditions, allowing for comprehensive and accurate data acquisition. Initial conditions of 3 bar and 333 K were used to mitigate contamination by stretch effects. Additionally, data for R1234yf were provided for extrapolation to standard conditions, enabling comparisons with literature data. Our results reveal substantial nonlinear blending effects on the laminar flame speed by introducing small fractions of R1234yf into R32 mixtures. While the selected kinetic model showed promising predictions, it could not fully predict the observed strong nonlinear flame speed decrease in experiments due to R1234yf addition. Chemical kinetic model analyses, including flux and sensitivity analyses, were employed to understand the blending interactions. The study highlights that the addition of R1234yf leads to the formation of HF, trapping radicals and inhibiting chain-branching reaction. Sensitivity analysis indicates that reactions involving fuel-specific radicals (CHF_2 for R32 and CF_3 for R1234yf) play a key role. Specifically, CHF_2 supplies H-atoms, while CF_3 drains H-atoms. Hence, the introduction of R1234yf leads to a reduction in flame temperature, the creation of an extended post-flame zone, and a substantial decrease in $S^0_{L,u}$.

1. Introduction

Refrigerants with a high global warming potential (GWP) are being replaced with low-GWP substitutes. The reduced atmospheric lifetimes, however, often come with mild flammability. Therefore, it is essential to understand their level of flammability. For safety evaluation, the laminar flame speed $S^0_{L,u}$ is an important property characterizing the combustion process. Compared to hydrocarbons, the amount of experimental and modeling studies on these hydroflurocarbon (HFC) refrigerants is sparse, making accurate experimental data extremely valuable for constraining uncertainties of chemical kinetic models. However, obtaining accurate data is also extremely challenging because of their often very low flame speeds.

Difluoromethane (CH_2F_2, R32) and 2,3,3,3-tetrafluoro-1-propene ($CH_2=CFCF_3$, R1234yf, short: "yf") are two low-GWP HFCs with estimated 100-year GWPs[1] of 809 and 1 (Hodnebrog et al. [1]), respectively. By mixing refrigerants, flammability, refrigerant cycle performance, stability, and low GWP properties can be tuned to obtain effective drop-in solutions for existing systems [2]. However, delineating the flammability characteristics of marginally flammable refrigerants and their blends is difficult. For example, R32 and R1234yf were reported by Takizawa et al. [3,4] with peak laminar flame speeds at standard conditions[2] of 6.7 cm/s and 1.2 cm/s, respectively. Accurate assessment of the combustion characteristics of these refrigerants places particular demands on laminar flame speed measurement methods.

☆ Official contribution of NIST, not subject to copyright in the United States. Certain commercial equipment, instruments, and materials are identified in this paper to adequately specify the procedure. Such identification does not imply recommendation or endorsement by the National Institute of Standards and Technology.

* Corresponding author.
E-mail address: r.hesse@itv.rwth-aachen.de (R. Hesse).

[1] GWP of CO_2 over 100 years used as reference.
[2] Standard conditions refer to 1.01325 bar and 298 K.

https://doi.org/10.1016/j.proci.2024.105418
Received 5 December 2023; Accepted 6 June 2024
Available online 10 July 2024

Due to the larger time scales of slowly propagating refrigerant flames, two physical phenomena dominate: (1) The buoyancy-induced deformation of the flames and (2) the radiation heat losses. These alter the flames not only on a kinematic but also on a chemical level and complicate flame speed estimates employing conventional methods. The flame speed of a refrigerant is analyzed in vertical cylindrical tubes (VT) made of glass, e.g., [5,6] or in closed combustion vessels (CV), e.g., [3,4,7,8]. The latter method determines $S^0_{L,u}$ by measuring the radius evolution of an outwardly propagating flame (OPF) using optical methods (O) such as Schlieren diagnostics or the pressure-rise trace (P) during the near isentropic compression phase. Available flame speed studies on R32 and R1234yf are summarized in the Supplementary Materials in Tab. S1. Only a minority of studies consider radiation effects with an optically thin gas model (OTM) and conduct experiments under microgravity (μg) to suppress buoyancy. Thus, chemical kinetic model development for HFC combustion prediction, e.g., by Papas et al. [6], Needham and Westmoreland [9], and Babushok et al. [10], partly relies on flame speed data, where radiation, buoyancy, and often stretch effects remain unconsidered. The present work addresses these challenges to provide accurate data. Much work was related to the flame propagation near the flammability limits, e.g., by Law and Egolfopoulos [11], Ju et al. [12], Bechtold et al. [13], and Chen and Ju [14]. These studies address the interplay of chain branching and breaking reactions [11], the transition to isolated self-extinguishing flames due to radiation [13,14], and the presence of radiation reabsorption in CO_2-dominated mixtures [12]. In the present work, flames do not self-extinguish because they are sufficiently far from the flammability limits, which is demonstrated by the optical and pressure-rise methods.

These two methods were compared in our previous study [8] addressing ambiguities in extracting the laminar flame speed for slowly propagating R32 flames under terrestrial (g) and microgravity (μg) conditions. By thoroughly identifying data reduction limits for optical and pressure-rise methods, flames with $S^0_{L,u}$ below 5 cm/s can be investigated, provided that effects of radiation heat losses are estimated and corrected. To effectively reduce stretch effects, experiments can be conducted at elevated pressures. These measures enable the acquisition of accurate data for kinetic model validation.

For this study, high-fidelity measurements were conducted to investigate the blending behavior of mixtures containing R32/R1234yf/air. To eliminate uncertainties arising from buoyancy, mixtures with R1234yf were measured under μg. The collected data provides a solid basis to answer the following questions: (1) How does the addition of R1234yf affect the flame speed of R32? (2) How can we describe the blending behavior? (3) What are the chemical processes occurring in these blends?

2. Experimental framework

Microgravity experiments were conducted in the high-repetition drop tower facility of ZARM (Center of Applied Space Technology and Microgravity) called the GraviTower Bremen Pro (GTB Pro) providing up to 2.5 s weightlessness of less than 10^{-4} g during drops. For details of the experimental setup, we refer to our previous descriptions [8]. Uncertainties were evaluated following the guide to the expression of uncertainty in measurement (GUM) [15]. The sensitivities of $S^0_{L,u}$ toward the input parameters, such as initial pressure, temperature, and mixture composition, were expressed with a simplified power law model representing the measured $S^0_{L,u}$. The expanded uncertainties for a level of confidence of 95 % are depicted as error bars in the results section figures. Brief descriptions of the experimental procedures and the uncertainty analysis are also included in the Supplementary Materials.

This study conducted experiments with dry air and molar R32/R1234yf blending ratios of $X_{yf} \in [0, 0.15, 0.3, 0.5, 1]$ and equivalence ratios of $\phi = 1.1$ and 1.3, which are expected to encompass peak flame speed positions, at a pressure of $p_0 = 3$ bar and a temperature of $T_0 = 333$ K. We previously reported peak laminar flame speeds for R32/air mixtures at $\phi = 1.05$ [16]. Takizawa et al. [4] identified a peak equivalence ratio for R1234yf/air at $\phi = 1.3$ and with oxygen-enriched air near 1.1. Thus, a variation in equivalence ratio of 1.1 to 1.3 should approximately cover peak $S^0_{L,u}$. Fuel-air equivalence ratio sweeps were conducted for pure R32 and R1234yf at the same initial pressure and temperature. In order to relate our findings at high pressures to standard conditions, we performed flame measurements of R1234yf/air for $\phi = 1.3$ along the isentropic compression line that corresponds to standard conditions. The collected flame speed data along this isentrope was used to determine the flame speed at standard conditions by extrapolation.

3. Flame speed determination

3.1. Optical method

Flame front extraction is limited to spherically smooth flame fronts above a critical radius associated with the complete decay of ignition artifacts and within a quasi-isobaric regime. The temporal evolution of the flame front radius (R_f) is measured at its iso-temperature surface of approximately 850 K using Schlieren images. Central differences are applied to obtain the stretched propagation speed of a burned mixture $S_{L,b} = \dot{R}_f = dR_f/dt$, assuming quiescent burned gases. The stretch rate K of an OPF is defined as the temporal change of the flame surface area A leading to $K = 1/A_f \cdot dA_f/dt = 2/R_f \cdot dR_f/dt$. The nonlinear expression provided by Kelley et al. [17] is used to calculate the unstretched flame speed $S^0_{L,b}$ denoted with the superscript "0" and the Markstein length $\mathcal{L}_b$. The unstretched laminar flame speed of the unburned gas, $S^0_{L,u}$, can be evaluated for adiabatic flames by mass continuity through a planar unstretched flame, $S^0_{L,u} = S^0_{L,b}(\rho_b/\rho_u)$, where ρ_b and ρ_u are the burned and unburned gas densities. A slowly burning flame can render the assumption of quiescent burned gases invalid due to radiation heat loss, inducing a contraction velocity (kinematic effect) and a temperature decrease in the reaction zone (chemical effect), as discussed by Hesse et al. [16]. Recently, Tavares et al. [18] improved the correction of the kinematic effect, emphasizing an important coupling of convective terms in the energy and continuity equations. The model predicts contraction velocities for R32 but deviates for R1234yf flames due to the slow oxidation of CO to CO_2, common in HFC flames with F/H > 1. Interpreting the larger fractions of CO in the burned gas as CO_2 leads to overestimating the radiation heat loss due to the larger Planck-mean absorption coefficients of CO_2. Their results imply that corrections of flame measurements under elevated pressures, which is the subject of the present study, are less affected because of their thinner reaction zone. Hence, corrections according to Tavares et al. are applied to optical method results.

3.2. Pressure-rise method

Several assumptions are invoked to calculate $S_{L,u}$ from pressure-rise data, including infinitely thin smooth spherical flame fronts during combustion, spatially uniform pressure during combustion, isentropic compression of unburned gases, ideal gases, equilibrium of burned gases, and negligible radiation and buoyancy effects. In Bariki et al. [19], we recently discussed this method and its errors in fast-burning flames using a two-zone model. For slowly burning flames, as investigated in the present study, a multi-zone model, such as the Mass- and Energy-Conserving Thermo (MECT) introduced by Elia et al. [20], is required to incorporate radiation heat losses. Here, we selected the data reduction tool for spherical constant volume flame experiments of the National Institute of Standards and Technology (NIST) [21], which uses the MECT multi-zone model. A detailed validation of the data reduction method and the aforementioned assumptions for slowly burning R32/air flames are presented by Hegetschweiler et al. [22]. Pressure data were processed by applying a moving average scheme. Radiation

effects were modeled in the burned equilibrated gas for the species CO_2, CO, H_2O, CF_2O, and HF, using the optically thin model (OTM), thus assuming the absence of radiation absorption. Handling radiation in a statistical narrow-band model framework is currently impossible due to the lack of radiation absorption parameters of some important species at appropriate combustion temperatures. It is important to recognize that experimental data obtained in the closed combustion vessel are always affected by radiation. In slowly propagating flames, correcting this data using a radiation model, e.g., OTM, is essential to compare results with adiabatic simulations. We label these corrected experimental results with 'rad-corr.' and the uncorrected results with 'uncorr.'.

A power law functional relationship is commonly used for extrapolating flame speeds to initial temperatures T_0 and pressures p_0, expressed as

$$S_{L,u} = S_{L,u,0}\left(\frac{p}{p_0}\right)^{\alpha}, \text{ and } \quad T = T_0\left(\frac{p}{p_0}\right)^{\frac{\gamma-1}{\gamma}}, \tag{1}$$

where $S_{L,u,0}$ is the laminar flame speed at p_0 and T_0, and the exponent α depends on the mixture composition. The corresponding temperature T along the near-isentropic compression is given by the second equation, with γ being the isentropic exponent with respect to the unburned gas.

3.3. Numerical framework

Flame speed simulations of adiabatic, planar stationary flames and transient spherically expanding flames were performed using the appropriate modules of the open-source code FlameMaster [23]. Predicted $S^0_{L,u}$ results shown in the following figures were obtained with the detailed kinetic model of Babushok et al. [24], which contains 113 species and 1064 reactions describing the combustion process of R32, R1234yf, and other C_2-C_3 HFC refrigerants.

4. Results and discussion

The reaction stoichiometry used to describe HFC/air (dry) mixtures in this study was defined by Takizawa et al. [25] for refrigerants containing equal or less fluorine than hydrogen atoms, e.g., R32 (CH_2F_2), and those containing more fluorine than hydrogen atoms, e.g., R1234yf (CH_2=$CFCF_3$), which are combined via the molar fraction X_{yf} of R1234yf in the refrigerant mixture:

$$\begin{aligned} &X_{yf} \cdot CH_2{=}CFCF_3 + (1 - X_{yf})\,CH_2F_2 + (1 + 1.5X_{yf})\,O_2 \\ &\quad = 2\,HF + X_{yf} \cdot CF_2O + (1 + X_{yf})\,CO_2. \end{aligned} \tag{2}$$

4.1. Optical method results

First, we analyzed the flame morphology of the optical measurements for all conditions. Fig. 1 depicts representative flame evolutions of R32 and R1234yf/air mixtures at an equivalence ratio of 1.1. R32/air flames propagate about three times faster than R1234yf/air flames, as indicated by the local propagation speeds $\dot{R}_f$ above the flame images.

Flames expand spherically without apparent artifacts caused by the electrodes. Although the present study was conducted at high ignition pressures of $p_0 = 3$ bar, flame wrinkling due to hydrodynamic or thermodiffusive instability is not an issue, as apparent from the optical flame evolution data. Particularly, it is not observed for richer flames of $\phi = 1.5$ and elevated pressures along the near-isentropic compression, relevant for pressure-rise data evaluation. Fig. 2 presents the relationship between the propagation speed $\dot{R}_f$ and the stretch rate K of the flame for both neat refrigerants and a blend of $X_{yf} = 0.15$ with $\phi = 1.1$, $p_0 = 3$ bar, and $T_0 = 333$ K. The data represented by symbols were corrected for radiation-induced contraction velocities using the code from Tavares et al. [18] and extrapolated using the nonlinear expression represented by lines to obtain the unstretched value. The flame propagation can be subdivided into three regimes associated

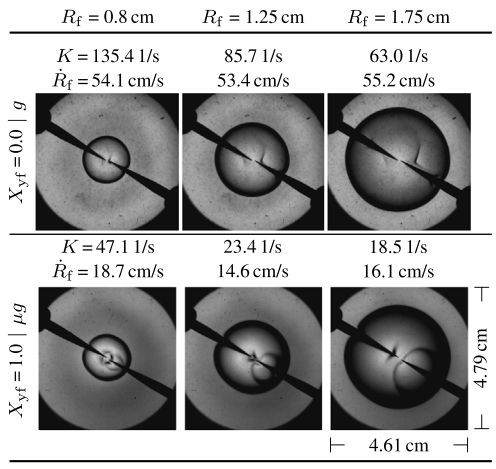

Fig. 1. Flame recordings at $\phi = 1.1$, $X_{O_2,air} = 20.94\,\%$, 333 K, and 3 bar at the volume equivalent radius R_f.

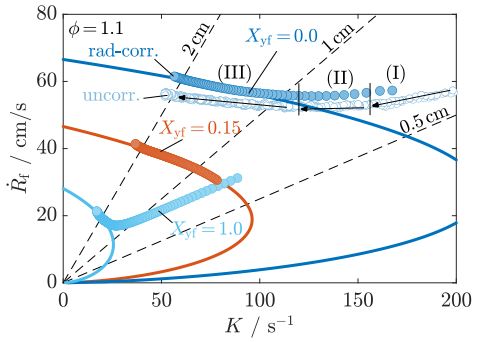

Fig. 2. Propagation speed-stretch rate dependence at 3 bar, 333 K, $\phi = 1.1$ with increasing R1234yf mole fraction X_{yf}. Filled symbols: radiation-corrected experiments; hollow symbols: uncorrected experiments; lines: nonlinear extrapolations; (I) ignition kernel propagation, (II) transition, and (III) normal flame propagation regime.

with (I) ignition energy decay, (II) transition to self-sustained propagation, (III) self-sustained flame propagation. Only (III) was selected for extrapolation to zero stretch rates.

Adding a fraction of $X_{yf} = 0.15$ to R32 drastically decreases the propagation speeds by 30 % and increases the Markstein length $\mathcal{L}_b$ from 0.9 mm to 1.4 mm. $\mathcal{L}_b$ further increases for neat R1234yf/air to 3.2 mm. These findings lead to a pronounced nonlinear blending behavior of $S^0_{L,u}$ for R1234yf-addition. The already large Markstein lengths for neat R1234yf/air flames at 3 bar and 333 K should be even larger for standard conditions, because $\mathcal{L}_b$ is proportional to the flame thickness, which increases toward lower pressures. Thus, the small optically accessible radius of about 2 cm in the present work makes extrapolations to zero stretch more uncertain, which is the reason why elevated pressures are beneficial in small combustion vessels, as discussed by Beeckmann et al. [26]. This also applies to the pressure-rise method, where stretch, ignition residues, and electrical noise can influence the lower data range.

4.2. Pressure-rise method results

The measured flame speeds from the pressure-rise method for the neat R1234yf/air mixtures at $\phi = 1.1$ are presented in Fig. 3. These flame speeds are already converted to the unburned conditions, so they are referred to as the laminar flame speed $S_{L,u}$. Note that $S_{L,u}$ is not strictly referring to the unstretched laminar flame speed $S^0_{L,u}$, as it might still be slightly stretch-affected at small flame radii and

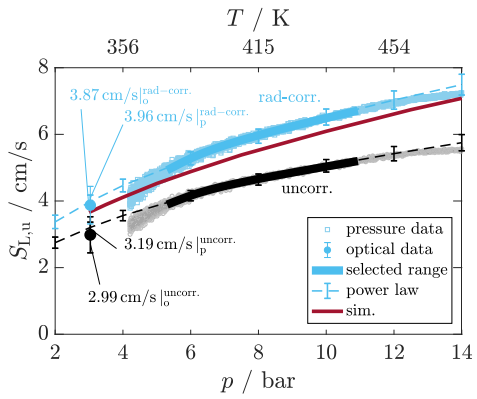

Fig. 3. $S_{L,u}$ of R1234yf/air (ϕ = 1.1) at $p_0 = 3$ bar, $T_0 = 333$ K, radiation-corrected and uncorrected, represented by blue and black points, respectively. Power law extrapolation to p_0 and T_0 (dashed lines) with error bars; Optical method results (filled points); Simulations (solid red line). (For interpretation of the references to color in this figure legend, the reader is referred to the web version of this article.)

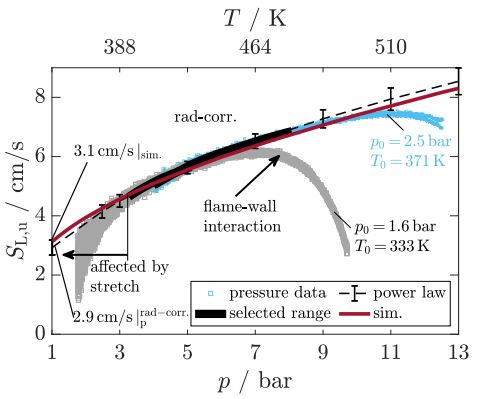

Fig. 4. $S_{L,u}$ of R1234yf/air (ϕ = 1.3) along near-isentropic compression lines corresponding to 1 atm and 298 K, with radiation correction; Initial condition: $p_0 = 1.6$ bar, $T_0 = 333$ K (black), and $p_0 = 2.5$ bar, $T_0 = 371$ K (light blue). (For interpretation of the references to color in this figure legend, the reader is referred to the web version of this article.)

corresponding low pressures. To prevent $S_{L,u}$ values from being contaminated by stretch effects, data must be selected and extrapolated to the initial conditions at p_0 and $T_{u,0}$. A lower limit of $p \gtrsim 1.4p_0$ to $2p_0$ was found to satisfy this demand for the present flames. The sensitive appropriate ranges for each case were assessed according to the procedures described by Hesse et al. [8] using the Markstein lengths from the optical data. For cross-validation, the extrapolated results to p_0 and T_0 from the pressure-rise evaluation (denoted with 'p') and $S^0_{L,u}$ from the optical evaluation (denoted with 'o') can be compared, as shown in Fig. 3. The upper limit for pressure data extrapolation is associated with the inflection point of the pressure–time history to exclude flame wall interactions. The symbols in Fig. 3, representing the extrapolated results, overlap due to the similarity of both method extrapolations, with the values from the pressure method being slightly higher than from the optical method. Equivalent visualizations to Figs. 2 and 3 for the other measurement conditions are provided in the Supplementary Materials.

To establish a connection between standard conditions that are typically used for fire-safety assessment of refrigerants, but are less precise to measure directly due to stretch effects, we conducted tests along the corresponding pressure and temperature isentrope for R1234yf/air mixtures with an equivalence ratio of 1.3. The results are shown in Fig. 4 for $p_0 = 1.6$ bar, $T_0 = 333$ K and $p_0 = 2.5$ bar, $T_0 = 371$ K. Data of multiple measurements overlap in the 3 bar to 5 bar range. For p and T below this range, data are affected by stretch since the flames are still too small and do not resemble a near-planar flame, which becomes apparent from the downward bend of the data points. After this range, measurements corresponding to $p_0 = 1.6$ bar are affected by flame wall interactions, whereas measurements conducted at $p_0 = 2.5$ bar provide reliable data up to 8 bar. Combining both sets and extrapolating them to standard conditions yields $S^0_{L,u} = 2.9$ cm/s. In comparison, Takizawa et al. [4] obtained 1.4 cm/s under μg without considering radiation and potentially large stretch effects.

Unstretched $S^0_{L,u}$ of the neat refrigerant/air mixtures as a function of the fuel-air equivalence ratio are shown in Fig. 5 for the two limiting cases, data reduction without correction (uncorr.) and including an OTM radiation-correction (rad-corr.). Estimated radiation effects are in the order of 14 % for peak R32/air flames to 40 % for rich R1234yf/air flames, with the uncorrected data being the reference. Data for R32 of the present study using the pressure-rise method are also compared to previous results by Hesse et al. [16] using radiation-corrected optical measurements. Measurement results are consistent up to an equivalence ratio of 1.4, where the new data are about 0.3 cm/s (6 %) slower, which is within the experimental uncertainties.

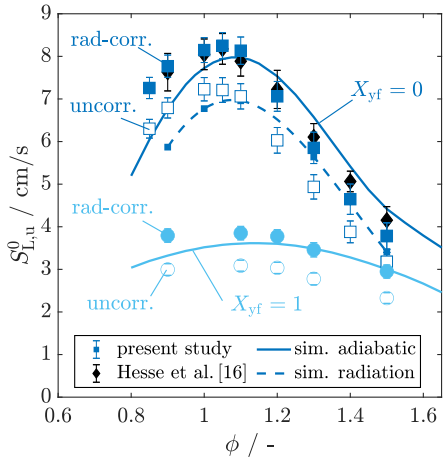

Fig. 5. $S^0_{L,u}$ of R32/air (dark blue) and R1234yf/air (light blue) over ϕ from the pressure-rise method at $p_0 = 3$ bar, $T_0 = 333$ K, radiation-corrected and uncorrected. Symbols: experiments; Solid lines: adiabatic planar stationary flame simulations; Dashed line: transient spherical flame simulations with OTM radiation for R32/air. (For interpretation of the references to color in this figure legend, the reader is referred to the web version of this article.)

Fig. 6 represents the blending behavior of the two refrigerants regarding their $S^0_{L,u}$ at $\phi = 1.1$. We observe a strong nonlinear behavior with increasing X_{yf}. For mixtures $X_{yf} \geq 0.5$, $S^0_{L,u}$ changes only within experimental uncertainty limits. A similar trend was reported by Takizawa et al. [7] as shown in the figure for peak velocities at standard conditions without radiation corrections. For comparison, Takizawa et al.'s results from [7] are also shown with radiation-heat losses estimated from the present study.

4.3. Predictions with the kinetic model

Fig. 5 compares radiation-corrected measurements (rad-corr.) to simulation results for several fuel-air equivalence ratios. For reference, uncorrected measurements representing a lower bound are included. The comparison illustrates the importance of accounting for radiation effects when validating kinetic model predictions against slow flame propagation data. Neglecting radiation may even lead to faulty conclusions about the prediction accuracy of a model, as is clear from the experimental results obtained for lean mixtures. The shape of the experimental and predicted results is well-matched for R32/air flame speeds. However, compared to the experiments, the predicted peak is shifted

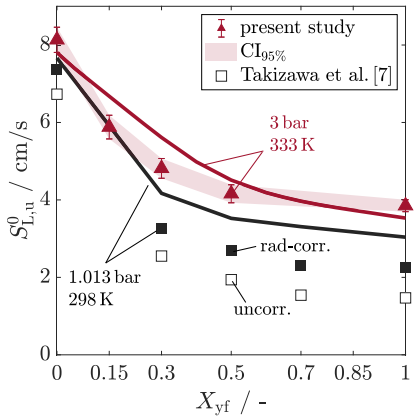

Fig. 6. $S^0_{L,u}$ blending effect of R32/air with R1234yf (X_{yf}) at $\phi = 1.1$, $p_0 = 3$ bar, $T_0 = 333$ K (red). Reference from Takizawa et al. [7] for blend peak velocities at $p_0 = 1.013$ bar, $T_0 = 298$ K (black), radiation-corrected and uncorrected. Symbols and lines show measured and computed results, respectively. (For interpretation of the references to color in this figure legend, the reader is referred to the web version of this article.)

so that $S^0_{L,u}$ is underpredicted on the lean side while slightly overpredicted for rich conditions. Deviations observed for mixtures leaner than $\phi = 1.0$ exceed the estimated experimental uncertainties and are attributed to kinetic model uncertainty. Flame speeds of R1234yf/air mixtures are underpredicted by the kinetic model for mixture leaner than $\phi = 1.3$.

Predictions for R1234yf/air mixtures along the isentropic compression lines in Figs. 3 and 4 are compared to radiation-corrected experiments. In the first case, at $p_0 = 3$ bar, $T_0 = 333$ K and $\phi = 1.1$, kinetic model predictions deviate from the experimental results' lower uncertainty range by 4 %. The pressure and temperature dependence of $S^0_{L,u}$ is matched by the simulations, as evident from the similar slope and curvature. Predictions for the richer second case along the isentropic compression line corresponding to standard conditions (cf. Fig. 4) are within experimental uncertainties for pressures and temperatures simultaneously increasing up to 12 bar and 520 K.

Lastly, the blending behavior of R1234yf in R32 is investigated numerically. Simulations show a similar nonlinear flame speed inhibition as experiments that levels off for $X_{yf} > 0.5$. For marginal R1234yf-addition, experiments indicate a more distinct flame speed inhibition than model predictions. The overall trend continues for standard conditions, which is in agreement with Takizawa et al.'s data [7]. Despite the retrospective radiation correction, Takizawa's absolute $S_{L,u}$ is not matched by the chemical kinetic model, which may originate from non-negligible stretch influence, as discussed in the previous section.

4.4. Reaction flux and sensitivity analysis

The qualitative flux diagram describing the consumption of R32 (CH_2F_2) and R1234yf (CH_2=$CFCF_3$) to form the products HF, CO_2, CF_2O, and CF_4 is shown in Fig. 7(a). The principal pathway for R32 involves the formation of the difluoromethyl radical CHF_2, which undergoes subsequent reactions with O and O_2 to yield fluoro-aldehydes. These aldehydes then decompose, producing HF and CO. In many aspects, difluoromethane pathways resemble methane oxidation, with fluorine replacing hydrogen atoms. In contrast, the fuel-specific chemistry of R1234yf forms (fluoro)-alkynes whose oxidation to aldehydes and subsequently CO relies on atomic oxygen due to the higher stability of the triple bonds. For both fuels, CO_2 is predominantly produced from oxidizing CO.

The fuel-specific systems of R32 and R1234yf are well-separated, except for two minor interactions. First, R1234yf consumption produces CF_3 radicals, which are subsequently oxidized to CF_2O. Second, R1234yf produces C_2HF, which reacts with atomic oxygen to form CHF biradicals. CF_4 acts as a fluorine sink, which becomes increasingly important for large F/H-ratio refrigerants, such as R1234yf. In contrast to the formation of CO_2, HF is more directly produced by the fuel-specific chemistry and partly by the reactions of fluoro-aldehydes.

Fig. 7(b) presents how the radical pool and $S^0_{L,u}$ change with X_{yf}. Peak radical molar fractions of H, OH, and CHF_2 decrease with a similar trend as $S^0_{L,u}$, whereas O first increases and then follows the trend of $S^0_{L,u}$. In all flames, O-atoms are predominantly produced by the reactions CHF + O_2 = CHFO + O and H + O_2 = O + OH. In a pure R32 flame, O-atom consumption occurs through reactions with R32 and its radical CHF_2. O-atom consumption decreases more rapidly than the O-production through the reaction CHF + O_2 = CHFO + O as R1234yf is added to the fuel, explaining the increasing O-atom mole fraction until reaching the peak O-atom mole fraction at X_{yf} = 0.15. For R1234yf, mole fractions larger than 0.15, the O-consumption through the reaction C_2HF + O = CO + CHF becomes increasingly important, which leads to an O-atom decrease. R1234yf-addition lowers the H-atom mole fraction via HF formation, effectively trapping the radicals and shutting down the chain branching, as explained below. Thus, fuel consumption must switch to the F-species radical-driven reactions, which are slower. The lack of available H-atoms also terminates conversions of F so that it remains an equilibrium product, as apparent from the strong rise in the post-reaction zone.

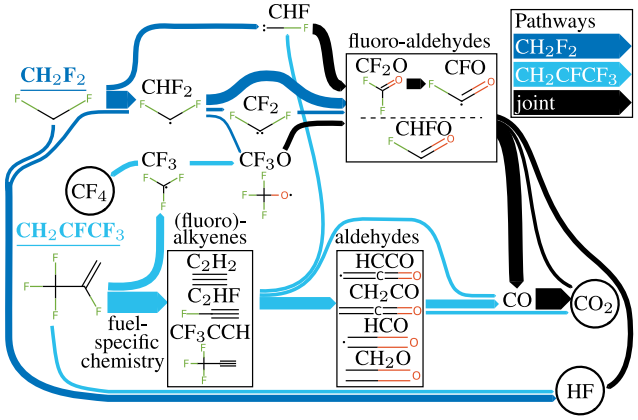

(a) Reaction flux diagram.

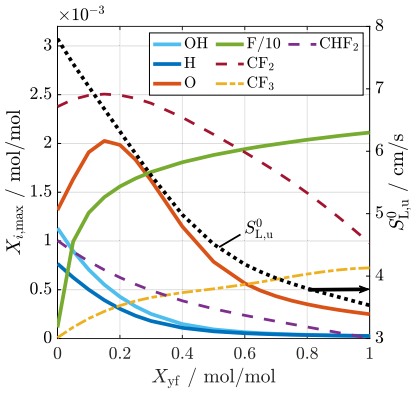

(b) Maximum radical pool.

Fig. 7. (a) Schematic reaction flux diagram for HF, CO_2, CF_2O, and CF_4 production. Dark blue pathways are attributed to R32 (CH_2F_2), light blue pathways to R1234yf (CH_2=$CFCF_3$), and black pathways to their joint chemistry in blends; (b) Maximum molar radical fraction (left y-axis) and $S^0_{L,u}$ (right y-axis) as function of X_{yf} for $\phi = 1.1$, 3 bar, and 333 K. Peak radical molar fractions are reached in the reaction zone, except for F (scaled by 1/10), which increases toward burned equilibrium.

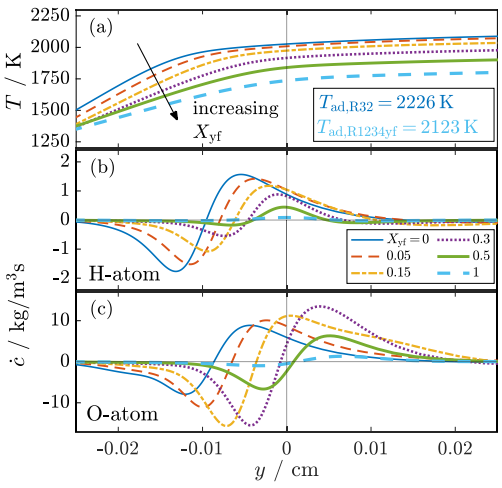

Fig. 8. (a) Temperature; (b) H production rate; (c) O production rate as a function of the flame coordinate y with the origin at OH peak concentration. Conditions are $p_0 = 3$ bar, $T_0 = 333$ K, and $\phi = 1.1$.

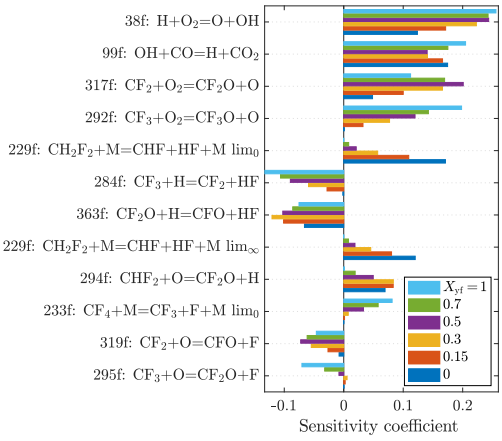

Fig. 9. Normalized sensitivity coefficients for $S^0_{L,u}$ with respect to frequency factors of rate coefficients at 3 bar, 333 K, $\phi = 1.1$, and varying X_{yf}.

As in hydrocarbon combustion, the laminar flame speed of fluorinated compounds is closely related to the flame temperature in the main reaction zone. The T-profiles for varying X_{yf} are depicted in Fig. 8(a). The length of the post-flame zone increases with X_{yf}. Differences in adiabatic flame temperatures between neat R32 and R1234yf are 103 K. However, the temperatures in the reaction layer vary significantly more by approximately 290 K (at $y = 0$). In Fig. 8(b), the net production rates $\dot{c}$ of H highlight not only the reduced amount of H radicals but also their withdrawal from the fuel-consumption region. Net production and consumption of O radicals, shown in Fig. 8(c), are also displaced toward larger flame coordinates. However, increasing X_{yf} first boosts O radicals before they decrease in mixtures with $X_{yf} > 0.3$.

Fig. 9 shows normalized sensitivity coefficients [27] for the laminar flame speeds of several fuel blends. All flame speeds are sensitive to the chain branching reaction 38f, which requires H-atoms to take place. Accordingly, the H-atom-producing reactions 99f and 294f increase $S^0_{L,u}$ while H-atom-consuming reactions, such as 284f and 363f, decrease it. In particular, the sensitivity coefficients of reactions 284f and 294f illustrate that the availability of H-atoms from fuel-specific intermediates impacts $S^0_{L,u}$ (CF_3 for R1234yf, CHF_2 for R32). In addition, the sensitivity analyses reveal that unimolecular decomposition reactions (229f and 233f) and reactions with O_2 and O (317f, 292f, 319f, 295f), which convert CF_3 and CF_2 to the product CF_2O, significantly affect $S^0_{L,u}$.

5. Concluding remarks

In the present study, we explored the nonlinear blending effect on the laminar flame speed of R1234yf and R32 mixtures by conducting high-fidelity experiments using the optical and pressure-rise methods under microgravity and terrestrial gravity and correcting results for radiation heat losses. To minimize contamination of $S^0_{L,u}$ values by stretch effects, we increased the initial conditions to pressure and temperature of 3 bar and 333 K. However, we also provided data for R1234yf that allows for robust extrapolation to standard conditions for comparison with literature data. This study underscores the necessity of implementing the aforementioned measures for slowly propagating flames to achieve experimental data accuracy suitable for refining kinetic models via comparisons to adiabatic, planar stationary flame simulations. Despite the promising predictions of the selected kinetic model for our measurements involving neat R32 and R1234yf, it was unable to completely account for the substantial nonlinear decrease in flame speed observed in the experiments. We analyzed the chemical kinetic model using flux and sensitivity analyses to understand the chemical interactions involved in blending these refrigerants. With R1234yf-addition, H-atoms react to form HF, trapping them and shutting down the typical hydrocarbon chain-branching reactions. Our sensitivity analysis highlights key reactions involving fuel-specific radicals: CHF_2 for R32, providing H-atoms, and CF_3 for R1234yf, removing H-atoms. Thus, R1234yf-addition has an attenuating effect on the flame temperature and produces an extended post-flame zone, which yields a strong decrease in $S^0_{L,u}$.

Novelty and Significance Statement

This research investigates the nonlinear flame speed inhibition effects in mixtures of R1234yf and R32, two hydrofluorocarbon refrigerants known for their low global warming potential but mild flammability, raising safety concerns. In our study, we employ high-fidelity experimental methods under microgravity conditions to overcome the challenges posed by these refrigerants' slow flame propagation. Added consideration of radiation and stretch effects, which were not jointly considered for R32/R1234yf/air mixtures before, provides accurate data for validating and improving kinetic models. Our experiments further highlight the significant flame speed inhibition potential of R1234yf in mixtures with R32. The detailed chemical kinetic model analyses reveal key steps in the oxidation chemistry of refrigerants. H-atoms enable reaction pathways that increase the laminar flame speed of R32. In contrast, R1234yf is oxidized via slower reactions with O_2 and O-atoms. This finding, explained in detail in this work, is essential in assessing refrigerant fire safety risks.

CRediT authorship contribution statement

Raik Hesse: Conceptualization, Methodology, Investigation, Analysis, Visualization, Writing – original draft. **Roman Glaznev:** Investigation, Data Analysis, Writing – review & editing. **Raymond Langer:** Analysis, Software, Data curation, Writing – original draft. **Christian Schwenzer:** Investigation, Data Analysis, Writing – review & editing. **Valeri Babushok:** Analysis, Scientific discussion. **Gregory Linteris:** Scientific discussion, Writing – review & editing. **Heinz Pitsch:** Supervision, Scientific discussion, Writing – review & editing. **Joachim Beeckmann:** Supervision, Funding acquisition, Scientific discussion, Writing – review & editing.

Declaration of competing interest

The authors declare that they have no known competing financial interests or personal relationships that could have appeared to influence the work reported in this paper.

Acknowledgments

R.H. and C.S. acknowledge the financial support provided by the Deutsches Zentrum für Luft und Raumfahrt (DLR, German Aerospace Center), Grant no. 50WM2258. R.G., J.B., and H.P. acknowledge the funding by the Deutsche Forschungsgemeinschaft (DFG, German Research Foundation) under Research Unit FOR 5507 with project number 497007546. Co-authors from NIST obtained financial support under contract DE-EE0007615 from the Office of Energy Efficiency and Renewable Energy, U.S. Department of Energy, and the U.S. Department of Defense, Strategic Environmental Research and Development Program (SERDP), under contract W74RDV91831838. We thank the European Space Agency (ESA) for funding and the Center of Applied Space Technology and Microgravity (ZARM) for contracting the drops in the GTB Pro.

Appendix A. Supplementary data

Supplementary material related to this article can be found online at https://doi.org/10.1016/j.proci.2024.105418.

References

[1] Ø. Hodnebrog, B. Aamaas, J.S. Fuglestvedt, G. Marston, G. Myhre, C.J. Nielsen, M. Sandstad, K.P. Shine, T.J. Wallington, Updated global warming potentials and radiative efficiencies of halocarbons and other weak atmospheric absorbers, Rev. Geophys. 58 (3) (2020) http://dx.doi.org/10.1029/2019RG000691.

[2] K. Thu, K. Takezato, N. Takata, T. Miyazaki, Y. Higashi, Drop-in experiments and exergy assessment of HFC-32/HFO-1234yf/R744 mixture with GWP below 150 for domestic heat pumps, Int. J. Refrig. 121 (2021) 289–301, http://dx.doi.org/10.1016/j.ijrefrig.2020.10.009.

[3] K. Takizawa, A. Takahashi, K. Tokuhashi, S. Kondo, A. Sekiya, Burning velocity measurement of fluorinated compounds by the spherical-vessel method, Combust. Flame 141 (3) (2005) 298–307, http://dx.doi.org/10.1016/j.combustflame.2005.01.009.

[4] K. Takizawa, K. Tokuhashi, S. Kondo, Flammability assessment of CH_2CFCF_3: Comparison with fluoroalkenes and fluoroalkanes, J. Hazard. Mater. 172 (2) (2009) 1329–1338, http://dx.doi.org/10.1016/j.jhazmat.2009.08.001.

[5] D. Clodic, T. Jabbour, Method of test for burning velocity measurement of flammable gases and results, HVAC&R Res. 17 (1) (2011) 51–75, http://dx.doi.org/10.1080/10789669.2011.543252.

[6] P. Papas, S. Zhang, W. Kim, S. Zeppieri, M. Colket, P. Verma, Laminar flame speeds of 2,3,3,3-tetrafluoropropene mixtures, Proc. Combust. Inst. 36 (1) (2016) 1145–1154, http://dx.doi.org/10.1016/j.proci.2016.06.073.

[7] K. Takizawa, Flammability assessment of CH_2=$CFCF_3$ (R-1234yf) and its mixtures with CH_2F_2 (R-32), in: Int. Symp. Next-Gen. Air-Con. Refrig. Technol, 2010.

[8] R. Hesse, C. Bariki, M.J. Hegetschweiler, G.T. Linteris, H. Pitsch, J. Beeckmann, Elucidating the challenges in extracting ultra-slow flame speeds in a closed vessel—A CH_2F_2 microgravity case study using optical and pressure-rise data, Proc. Combust. Inst. 39 (2022) http://dx.doi.org/10.1016/j.proci.2022.07.167.

[9] C. Needham, P. Westmoreland, Combustion and flammability chemistry for the refrigerant HFO-1234yf (2, 3 3, 3-tetrafluoropropene), Combust. Flame 184 (Supplement C) (2017) 176–185, http://dx.doi.org/10.1016/j.combustflame.2017.06.004.

[10] V. Babushok, D. Burgess, D. Kim, M. Hegetschweiler, G. Linteris, Modeling of Combustion of Fluorine-Containing Refrigerants, NIST Tech. Note 2170, 2021, http://dx.doi.org/10.6028/NIST.TN.2170.

[11] C. Law, F. Egolfopoulos, A unified chain-thermal theory of fundamental flammability limits, Symp. (Int.) Combust. 24 (1) (1992) 137–144, http://dx.doi.org/10.1016/S0082-0784(06)80021-4.

[12] Y. Ju, G. Masuya, P.D. Ronney, Effects of radiative emission and absorption on the propagation and extinction of premixed gas flames, Symp. (Int.) Combust. 27 (2) (1998) 2619–2626, http://dx.doi.org/10.1016/S0082-0784(98)80116-1.

[13] J. Bechtold, C. Cui, M. Matalon, The role of radiative losses in self-extinguishing and self-wrinkling flames, Proc. Combust. Inst. 30 (1) (2005) 177–184, http://dx.doi.org/10.1016/j.proci.2004.07.031.

[14] Z. Chen, Y. Ju, Theoretical analysis of the evolution from ignition kernel to flame ball and planar flame, Combust. Theor. Model. 11 (3) (2007) 427–453, http://dx.doi.org/10.1080/13647830600999850.

[15] JCGM, Evaluation of measurement data — Guide to the expression of uncertainty in measurement, 2008, https://ncc.nesdis.noaa.gov/documents/documentation/JCGM_100_2008_E.pdf.

[16] R. Hesse, L. Berger, C. Bariki, M.J. Hegetschweiler, G.T. Linteris, H. Pitsch, J. Beeckmann, Low global-warming-potential refrigerant CH_2F_2 (R-32): Integration of a radiation heat loss correction method to accurately determine experimental flame speed metrics, Proc. Combust. Inst. 38 (3) (2020) 4665–4672, http://dx.doi.org/10.1016/j.proci.2020.05.026.

[17] A. Kelley, J. Bechtold, C. Law, Premixed flame propagation in a confining vessel with weak pressure rise, J. Fluid Mech. 691 (2012) 26–51, http://dx.doi.org/10.1017/jfm.2011.439.

[18] J.K. Tavares, V. Gururajan, J. Jayachandran, Effects of radiation heat loss on planar and spherical hydrofluorocarbon/air flames, Combust. Flame 258 (2023) 113067, http://dx.doi.org/10.1016/j.combustflame.2023.113067.

[19] C. Bariki, R. Hesse, F. Halter, H. Pitsch, J. Beeckmann, Combined isochoric and isobaric acquisition methodology for accurate flame speed measurements from ambient to high pressures and temperatures, Proc. Combust. Inst. 38 (2) (2020) 2185–2193, http://dx.doi.org/10.1016/j.proci.2020.08.003.

[20] M. Elia, M. Ulinski, M. Metghalchi, Laminar burning velocity of Methane–Air–Diluent mixtures, J. Eng. Gas Turbines Power 123 (1) (2000) 190–196, http://dx.doi.org/10.1115/1.1339984.

[21] M. Hegetschweiler, G.T. Linteris, Data Reduction Tool for Spherical Constant Volume Flame Experiments, NIST Tech. Note 2148, 2021, http://dx.doi.org/10.6028/NIST.TN.2148.

[22] M.J. Hegetschweiler, L. Berger, R. Hesse, J. Beeckmann, C. Bariki, H. Pitsch, G.T. Linteris, Data reduction considerations for the burning velocity of spherical constant volume flames of R32 (CH_2F_2) with air, Combust. Flame 254 (2023) 112807, http://dx.doi.org/10.1016/j.combustflame.2023.112807.

[23] H. Pitsch, R. Langer, Flamemaster: A C++ computer program for 0D combustion and 1D laminar flame calculations, 2023, https://www.itv.rwth-aachen.de/downloads/flamemaster/, version 4.4.0.

[24] V. Babushok, D. Burgess Jr., M. Hegetschweiler, G. Linteris, Flame propagation in the mixtures of O_2/N_2 oxidizer with fluorinated propene refrigerants (CH_2CFCF_3, $CHFCHCF_3$, CH_2CHCF_3), Combust. Sci. Technol. (2020) 1–24, http://dx.doi.org/10.1080/00102202.2020.1720663.

[25] K. Takizawa, A. Takahashi, K. Tokuhashi, S. Kondo, A. Sekiya, Reaction stoichiometry for combustion of fluoroethane blends, ASHRAE Trans. 112 (2) (2006) 459–469.

[26] J. Beeckmann, R. Hesse, J. Schaback, H. Pitsch, E. Varea, N. Chaumeix, Flame propagation speed and markstein length of spherically expanding flames - assessment of extrapolation and measurement techniques, Proc. Combust. Inst. 37 (2019) 1521–1528, http://dx.doi.org/10.1016/j.proci.2018.08.047.

[27] R. Langer, J. Lotz, L. Cai, F. vom Lehn, K. Leppkes, U. Naumann, H. Pitsch, Adjoint sensitivity analysis of kinetic, thermochemical, and transport data of nitrogen and ammonia chemistry, Proc. Combust. Inst. 38 (2021) 777–785, http://dx.doi.org/10.1016/j.proci.2020.07.020.